REPORT DOCUMENTATION PAGE

Form Approved
OMB No. 0704-0188

1. REPORT DATE *(DD-MM-YYYY)*	2. REPORT TYPE	3. DATES COVERED *(From - To)*
31-10-2005	Journal Article	

4. TITLE AND SUBTITLE

Theory of Monte-Carlo Simulations of the Magnetic Circular Dichroism (MCD) Spectra of Alkali Metal/Rare Gas Systems (PREPRINT)

5a. CONTRACT NUMBER

5b. GRANT NUMBER

5c. PROGRAM ELEMENT NUMBER

6. AUTHOR(S)

John W. Kenney (Concordia University); Jerry A. Boatz (AFRL/PRSP); Heidi A. Terrill Vosbein (Stennis Space Center)

5d. PROJECT NUMBER
23030423

5e. TASK NUMBER

5f. WORK UNIT NUMBER

7. PERFORMING ORGANIZATION NAME(S) AND ADDRESS(ES)

Air Force Research Laboratory (AFMC)
AFRL/PRSP
10 E. Saturn Blvd.
Edwards AFB CA 93524-7680

8. PERFORMING ORGANIZATION REPORT NUMBER

AFRL-PR-ED-JA-2005-439

9. SPONSORING / MONITORING AGENCY NAME(S) AND ADDRESS(ES)

Air Force Research Laboratory (AFMC)
AFRL/PRS
5 Pollux Drive
Edwards AFB CA 93524-7048

10. SPONSOR/MONITOR'S ACRONYM(S)

11. SPONSOR/MONITOR'S NUMBER(S)
AFRL-PR-ED-JA-2005-439

12. DISTRIBUTION / AVAILABILITY STATEMENT

Approved for public release; distribution unlimited (AFRL-ERS-PAS-2005-277)

13. SUPPLEMENTARY NOTES

Submitted for publication in the International Journal of Quantum Chemistry

14. ABSTRACT

The history of magnetic circular dichroism (MCD) spectroscopy in the study of alkali metal/rare gas (M/Rg) cryogenic systems is reviewed in the context of developing a better understanding of alkali metal/hydrogen systems of current interest to the U.S. Air Force as enhanced-performance cryogenic rocket propellants. A new theory for simulating the MCD spectra of M/Rg systems is presented together with a careful discussion of the theory's implicit and explicit approximations and their implications.

15. SUBJECT TERMS

16. SECURITY CLASSIFICATION OF:			17. LIMITATION OF ABSTRACT	18. NUMBER OF PAGES	19a. NAME OF RESPONSIBLE PERSON
a. REPORT	b. ABSTRACT	c. THIS PAGE			Dr. Scott A. Shackelford
Unclassified	**Unclassified**	**Unclassified**	A	24	19b. TELEPHONE NUMBER *(include area code)* N/A

Theory of Monte-Carlo simulations of the Magnetic Circular Dichroism (MCD) spectra of alkali metal/rare gas systems

John W. Kenney, III

Chemical Physics Laboratory, Concordia University,

1530 Concordia West, Irvine, CA 92612

Jerry A. Boatz

Air Force Research Laboratory, Space and Missle Propulsion Division; AFRL/PRSP,

10 E. Saturn Blvd., Edwards AFB, CA 93524

Heidi A. Terrill Vosbein

Naval Research Laboratory, Acoustic Simulation,

Measurements and Tactics Branch, Code 7180,

Bldg. 1005, Stennis Space Center, MS 39529

(Dated: ; Received text ; Revised text ;

Accepted text ; Published text)

Abstract

The history of magnetic circular dichroism (MCD) spectroscopy in the study of alkali metal/rare gas (M/Rg) cryogenic systems is reviewed in the context of developing a better understanding of alkali metal/hydrogen systems of current interest to the U.S. Air Force as enhanced-performance cryogenic rocket propellants. A new theory for simulating the MCD spectra of M/Rg systems is presented together with a careful discussion of the theory's implicit and explicit approximations and their implications. This theory uses a classical Monte Carlo (MC) simulation scheme to model the perturbing effects of the Rg environment on the $^2S \rightarrow {}^2P$ MCD-active transition of the M atom. The theory sets up the MC-MCD simulation as a 6×6 matrix eigenvalue/eigenvector problem in the ^2P manifold in which is included the effects of M-Rg interactions, metal atom spin-orbit coupling in the ^2P manifold, magnetic Zeeman perturbations of the ^2S and ^2P manifolds, Boltzmann temperature factors, and electric dipole transition moment integrals for left circularly polarized (LCP) and right circularly polarized (RCP) light. The theory may be applied to any type of trapping site of the host M in the guest Rg matrix; a single atom substitutional metal atom trapping site (one host Rg atom is replaced by one guest M atom) is modeled in this study for M = Na and Rg = Ar. Two temperature factors are used in these simulations; a lattice temperature to model the mobility of the Rg lattice and a magnetic temperature to model Boltzmann factors in the ^2S ground manifold. The 6×6 eigenvalue/eigenvector problem is solved for a number of randomly generated and suitably averaged Rg configurations to yield the simulated MC-MCD spectrum for the single substitutional Na/Ar system. The MC-MCD simulations of Na/Ar give the characteristic triplet MCD spectrum with the correct Boltzmann temperature dependence. The simulated MC-MCD spectrum correctly inverts when the direction of the applied magnetic field is reversed. Addition of the LCP and RCP absorbances gives rise to a characteristic $^2S \rightarrow {}^2P$ triplet absorption feature.

Contents

I. INTRODUCTION

Alkali metal/rare gas solids (M/Rg solids) constitute an important class of model systems of interest to the U. S. Air Force in simulating the properties of enhanced-performance cryogenic rocket propellants [1–4]. In particular, the alkali metal/rare gas (M/Rg) systems share many physical, chemical, and spectroscopic characteristics with M/hydrogen systems, where in a potential rocket propulsion application, M is a high energy density material (HEDM); e.g., a low mass alkali metal or Group 13 or 14 element [5, 6]. Boatz and Fajardo recently modeled $^2S \rightarrow {}^2P$ electronic absorption spectra in M/Rg systems by using quantum mechanical first-order degenerate perturbation theory in conjunction with a classical Monte Carlo (MC) method to account statistically for the effects of the Rg perturbations on the ^2S and ^2P terms of the M/Rg systems [7]. Their simulations, while not

completely quantitative, do recover many of the key attributes of the electronic absorption spectra of these systems including the characteristic three-peaked or "triplet" absorption band shape. Lawrence and Apkarian take a very similar approach in modeling the ^2P terms of halogen atoms doped in cryrogenic matrices (X/Rg) [8]. Boatz and Fajardo make the reasonable assumption that spin-orbit coupling represents a small perturbation of the ^2P term compared to the Rg perturbation, at least for the lighter alkali metals of interest to them as HEDM rocket propellant dopants, and on this basis justify the exclusion of ^2P spin-orbit coupling terms in their model. The Boatz and Fajardo first-order perturbation matrix for the ^2P term is, therefore a 3×3 matrix whose matrix elements are defined with respect to a suitable zeroth-order orbital p basis in the angular momentum representation ($|n\ l\ m_l\rangle = |n\ 1\ 1\rangle$,$|n\ 1\ 0\rangle$,$|n\ 1\ -1\rangle$). Spin is not considered. Lawrence and Apkarian do include a ^2P spin-orbit term for the halogen in their treatment. They argue convincingly that the large halogen ^2P spin-orbit coupling interaction is not greatly affected by the matrix environment, i.e., the use of the atomic spin-orbit coupling constant of the halogen in the formalism represents a good approximation. The Lawrence and Apkarian ^2P perturbation matrix is a 6×6 matrix whose individual matrix elements are defined with respect to a suitable zeroth-order Cartesian p basis with spin $\{|n\ l\ e\ s\ m_s\rangle = \left|n\ l\ x\ \frac{1}{2}\ \frac{1}{2}\right\rangle$, $\left|n\ l\ y\ \frac{1}{2}\ \frac{1}{2}\right\rangle$, $\left|n\ l\ z\ \frac{1}{2}\ \frac{1}{2}\right\rangle$, $\left|n\ l\ x\ \frac{1}{2}\ -\frac{1}{2}\right\rangle$, $\left|n\ l\ y\ \frac{1}{2}\ -\frac{1}{2}\right\rangle$, $\left|n\ l\ z\ \frac{1}{2}\ -\frac{1}{2}\right\rangle\}$.

Magnetic circular dichroism (MCD) spectroscopy, which measures the differential absorption of left circularly polarized (LCP) light vs. right circularly polarized (RCP) light in a sample placed in a magnetic field aligned parallel to the propagation direction of the light, has a long and venerable history of providing insights to the nature of the chemical and physical environment surrounding the MCD-active chromophore [9]. In particular, the MCD-active $^2S \rightarrow {}^2P$ electronic transitions of alkali halide F centers [10–14] and M/Rg systems [15–18] have attracted considerable experimental and theoretical attention over the years. The usual approach is to extract parameters such as the g value, the spin-orbit coupling constant, and linear vibrational coupling constants from a moment analysis of the experimental MCD spectrum (or spectra) [9, 11]. Only a few full MCD spectral simulations exist in the literature. These simulations of $^2S \rightarrow {}^2P$ MCD spectra rely upon dynamic Jahn-Teller models in which an a priori choice is made as to which specific interaction vibrational modes will act to lift the degeneracy of the ^2P term [19, 20]. This simulation approach is of limited value in modeling the MCD spectra of M atoms trapped in novel

and heretofore unobserved sites in Rg matrices for which specific site geometries and lattice mode types are as yet unknown. A MC approach for handling Rg perturbations in MCD simulations of M/Rg systems naturally suggests itself. A full development of the theory of Monte Carlo-MCD (MC-MCD) simulations of $^2S \rightarrow {}^2P$ MCD spectra is presented in the sections that follow. The MC-MCD simulation method is a first order degenerate perturbation method that straightforwardly extends the MC absorption- simulation methods of Boatz and Fajardo [7] and Lawrence and Apkarian [8] by (1) including both spin-orbit and Zeeman perturbations in the Hamiltonian and (2) separately treating the $^2S \rightarrow {}^2P$ transitions associated with LCP and RCP light. The MC-MCD perturbation matrix for the ^2P term is a 6×6 matrix whose individual matrix elements are expressed in terms of a suitable uncoupled angular momentum p basis set with spin $\{|n\,l\,m_l\,s\,m_s\rangle = \left|n\,1\,1\,\frac{1}{2}\;\frac{1}{2}\right\rangle$, $\left|n\,1\,0\,\frac{1}{2}\,\frac{1}{2}\right\rangle$, $\left|n\,1\;-1\;\;\frac{1}{2}\,\frac{1}{2}\right\rangle$, $\left|n\,1\,1\,\frac{1}{2}\;-\frac{1}{2}\right\rangle$, $\left|n\,1\,0\,\frac{1}{2}\;-\frac{1}{2}\right\rangle$, $\left|n\,1\;-1\;\;\frac{1}{2}\;-\frac{1}{2}\right\rangle\}$.

II. THEORY

As noted above, the theory of MC-MCD spectroscopy of $^2S \rightarrow {}^2P$ excitations in M/Rg systems represents an extension of the formalism for MC-absorption spectroscopy developed by Boatz and Fajardo [7] (for M/Rg systems) and Lawrence and Apkarian [8] (for X/Rg systems). Key aspects of both the Boatz and Fajardo and Lawrence and Apkarian notational schemes are adopted in the following formal development.

A. Total Hamiltonian and zeroth-order eigenvectors/eigenvalues

The total Hamiltonian for an alkali metal M atom imbedded in a cryogenic rare gas matrix comprised of N Rg atoms in the presence of an applied external magnetic field is given by

$$H = H_M(\mathbf{r}) + H_{int}(\mathbf{r}; \mathbf{R}_1, \mathbf{R}_2, ..., \mathbf{R}_N), \tag{1}$$

where

$$H_M(\mathbf{r}) = T_M(\mathbf{r}) + V_M(\mathbf{r}) \tag{2}$$

is the one-electron Hamiltonian for the optically active electron on M at position r, comprised of a kinetic energy component $T_M(\mathbf{r})$ and an electrostatic potential energy component $V_M(\mathbf{r})$.

The potential $V_M(\mathbf{r})$ is the potential experienced by the optically active electron in the free gas-phase M atom in the absence of spin-orbit coupling or an external magnetic field.

To describe completely the ^2S ground term of M, two zeroth-order eigenvectors $\{|n\,0\,0\,\frac{1}{2}\,m_s\rangle;\ m_s = 1/2.\ \text{-}1/2)$ are needed; for the ^2P excited term, six zeroth-order eigenvectors $\{|n\,l\,m_l\,s\,m_s\rangle;\ m_l. = 1,\ 0,\ \text{-}1,\ m_s = 1/2,\ \text{-}1/2\}$ are required. An uncoupled angular momentum representation $\{|n\,l\,m_l\,s\,m_s\rangle\}$ for the zeroth-order eigenvectors is chosen, without loss of generality, because of the transparent way in which MCD selection rules may be expressed in terms of this representation (*vide infra*). However, it is equally valid to use zeroth-order eigenvector sets expressed in the coupled angular momentum representation $\{|n\,l\,s\,j\,m\rangle$ or the Cartesian representation $\{|n\,l\,e\,s\,m_s\rangle\}$ ($e = x, y, z$ for $l = 1$) since the uncoupled, coupled, and Cartesian representations are mutually related by unitary transformations [21]. In this treatment, the interaction Hamiltonian is comprised of four terms, each of which depends upon the nuclear position vectors $\{R_k\}$of all of the N Rg atoms in the matrix; a metal-rare gas interaction term, a rare gas-rare gas interaction term, a spin-orbit term, and a Zeeman term,

$$H_{int}(\mathbf{r};\mathbf{R}_1,\mathbf{R}_2,...,\mathbf{R}_N) = V_{M-Rg}(\mathbf{r};\mathbf{R}_1,\mathbf{R}_2,...,\mathbf{R}_N) + V_{Rg-Rg}(\mathbf{r};\mathbf{R}_1,\mathbf{R}_2,...,\mathbf{R}_N) + H_{so}(\mathbf{r};\mathbf{R}_1,\mathbf{R}_2,...,\mathbf{R}_N) + H_{Zeeman}(\mathbf{r};\mathbf{R}_1,\mathbf{R}_2,...,\mathbf{R}_N) \quad (3)$$

The M nucleus is taken to be the origin of the coordinate system with respect to which r and the $\{R_k\}$ are defined. In this treatment, it is assumed, following Lawrence and Apkarian, that M-Rg interactions do not affect Rg-Rg interactions [8]; no modifications have been made to the Rg-Rg potentials to account for perturbations arising from the presence of the M atom.

B. The Rg-Rg and M/Rg potentials

The Rg-Rg interaction potential in Eq. 3 can be approximated as a simple sum over the appropriate S symmetry Rg-Rg diatomic potentials

$$V_{Rg-Rg}(\mathbf{R}_1,\mathbf{R}_2,...,\mathbf{R}_N) = \sum_{m=1,N}\sum_{m<k} V_{Rg-Rg}(|\mathbf{R}_m - \mathbf{R}_k|) = U_{Rg-Rg} \quad (4)$$

following the notation of Boatz and Fajardo [7]. It should be noted that U_{Rg-Rg} has the same value for both the ^2S and ^2P terms at this level of approximation.

The M-Rg potential, which in general exhibits a complicated dependence upon the Rg positions (R_k), is expressed in terms of a Legendre polynomial expansion as

$$V_{M-Rg}(\mathbf{r};\mathbf{R}_1,\mathbf{R}_2,...,\mathbf{R}_N) = \sum_{k=1,N}\sum_{L=0,infinity} V_L(\mathbf{r},\mathbf{R}_k)P_L(\theta,\phi;\theta_k,\phi_k) \tag{5}$$

where $\mathbf{r} = (r,\theta,\phi)$ is the optically active electron position vector, $\mathbf{R}_k = (R_k,\theta_k,\phi_k)$ is the position vector for Rg nucleus k. $V_L(\mathbf{r},\mathbf{R}_k)$ is the radial potential function of order L, and $P_L(\theta,\phi;\theta_k,\phi_k)$ is the Legendre polynomial of order L

$$P_L(\theta,\phi;\theta_k,\phi_k) = 4\pi(2L+1)^{-1}\sum_{M=-L,L} Y_{LM}(\theta,\phi)Y^*_{LM}(\theta_k,\phi_k) \tag{6}$$

and the Y_{LM} are spherical harmonic functions expressed in the standard Condon and Shortley phase convention [22]. Eq. 6 is an expression of one of the possible forms of the spherical harmonic addition theorem [21].

C. Spin-orbit coupling operator

The spin-orbit coupling operator for the optically active electron may be written, using the standard defining equation for the spin-orbit interaction [23], in terms of the potential gradient of the free M and M-Rg interaction potentials

$$\begin{aligned} H_{so}(\mathbf{r};\mathbf{R}_1,\mathbf{R}_2,...,\mathbf{R}_N) &= H_{so,M}(\mathbf{r}) + H_{SO,M-Rg}(\mathbf{r};\mathbf{R}_1,\mathbf{R}_2,...,\mathbf{R}_N) \\ &= \{(2me^2c^2r)^{-1}\nabla[V_M(\mathbf{r}) + V_{M-Rg}(\mathbf{r};\mathbf{R}_1,\mathbf{R}_2,...,\mathbf{R}_N)]\times\mathbf{p}\}\cdot\mathbf{S} \\ &= [\xi_M(r) + \xi_{M-Rg}(r)]\mathbf{L}\cdot\mathbf{S} + [(2me^2c^2r)^{-1} \\ &\quad \times\nabla\{\sum_{k=1,N}\sum_{L=1,infinity} V_L(\mathbf{r},\mathbf{R}_k)P_L(\theta,\phi;\theta_k,\phi_k)\}\times\mathbf{p}]\cdot\mathbf{S} \end{aligned} \tag{7}$$

where $\mathbf{p}$ and $\mathbf{S}$ are, respectively, the linear momentum and spin operators for the optically active electron, $\mathbf{L} = \mathbf{r}\times\mathbf{p}$ is the angular momentum operator for the optically active electron and

$$\xi_M(r) = (2me^2c^2r)^{-1}d[V_M(\mathbf{r})]/dr \tag{8}$$

is the standard spin-orbit coupling operator for the free M atom. The M-Rg interaction potential of Eq. 5 can be broken up into spherical and non-spherical components

$$V_{M-Rg}(\mathbf{r};\mathbf{R}_1,\mathbf{R}_2,...,\mathbf{R}_N) = \sum_{k=1,N} V_0(\mathbf{r},\mathbf{R}_k) + \sum_{k=1,N}\sum_{L=1,infinity} V_L(\mathbf{r},\mathbf{R}_k)P_L(\theta,\phi;\theta_k,\phi_k). \tag{9}$$

In the form of the theory currently in use for MC-MCD simulations, it is assumed that the gradient expression in Eq. 7 is small and can be neglected; i.e., no $L > 0$ terms are assumed to contribute to the spin-orbit coupling interaction. The total spin-orbit coupling operator of the M/Rg system in the spherical approximation is thus given by

$$H_{so}(\mathbf{r}) = H_{so,M}(\mathbf{r}) + H_{SO,M-Rg}(\mathbf{r}) = [\xi_M(r) + \xi_{M-Rg}(r)]\mathbf{L}\cdot\mathbf{S} = \xi(r, \mathbf{L}\cdot\mathbf{S}) \qquad (10)$$

where the dependence on the Rg position vectors $\{R_k\}$, while present is not explicitly shown in the interest of preserving a compact notation in the final form of the equations used.

No spin-orbit coupling is possible when the optically active electron is in the ^2S ground state manifold where $l = 0$. In the ^2P excited state manifold where $l = 1$, the spin-orbit coupling constant is expressed formally as the sum of the radial expectation values of the spherically symmetric M and M-Rg spin-orbit coupling operators

$$\zeta_{nl} = \langle n\ l|\, \xi(r)\, |n\ l\rangle = \langle n\ l|\, \xi_M(r)\, |n\ l\rangle + \langle n\ l|\, \xi_{M-Rg}(r)\, |n\ l\rangle = \zeta_M + \zeta_{M-RG} \qquad (11)$$

If the radial eigenvector $|n\ l\rangle$ is the free atom P state atomic radial eigenvector for M, or if $|n\ l\rangle$ closely approximates this eigenvector, then ζ_M is the free alkali atom spin-orbit coupling constant and ζ_{M-RG} is the spherical perturbation to the spin-orbit coupling constant induced in M by the Rg matrix environment. Eq. 11 provides an insightful context for discussing the possibilities of (1) spin-orbit coupling constant sign reversal or (2) reduction of the magnitude of a spin-orbit coupling constant (partial quenching, in a ^2P M-Rg system. For any given alkali metal M the free atom ^2P spin-orbit coupling constant is positive; i.e., $\zeta_M > 0$. Thus, for a ^2P spin-orbit coupling constant ζ_{nl} to be negative in a M-Rg system, the M-Rg spin orbit contribution must be negative and larger in magnitude than the free M atom spin-orbit coupling constant. i.e., $\zeta_{M-RG} < 0$ and $|\zeta_{M-RG}| > \zeta_M$ The conditions for the partial quenching case, where ζ_{nl} is still positive but smaller than ζ_M are: $\zeta_{M-RG} < 0$ and $|\zeta_{M-RG}| < \zeta_M$. In the actual MC-MCD simulations, ζ_{nl} is introduced as an adjustable parameter. The two cases may be explored in the MC-MCD simulations by making appropriate choices for ζ_{nl} with respect to the known positive ζ_M of the alkali metal M atom of interest.

D. Zeeman Perturbation

The Zeeman perturbation operator is given by

$$H_{Zeeman}(\mathbf{r}; \mathbf{R}_1, \mathbf{R}_2, ..., \mathbf{R}_N) = \mu_B \mathbf{B}_{local}(\mathbf{L} + 2\mathbf{S}) \qquad (12)$$

where μ_B is the Bohr magneton, $\mathbf{L}$ and $\mathbf{S}$ are the orbital and spin angular momentum operators for the optically active electron, and $\mathbf{B}_{local}$ is the magnetic field locally experienced by the optically active electron as a result of the application of an external magnetic field B to the M/Rg system. Both the magnitude and the direction of the local magnetic field vector are influenced by the positions of the Rg atoms and by the nature of the electronic state of the optically active electron (i.e., ^2S or ^2P). The relationship between the external magnetic field and the local magnetic field thus may be expressed as

$$\mathbf{B}_{local} = \mathbf{B}_{local}(\mathbf{R}_1, \mathbf{R}_2, ..., \mathbf{R}_N) = [1 - \sigma_{nl}(\mathbf{R}_1, \mathbf{R}_2, ..., \mathbf{R}_N)]\mathbf{B} \tag{13}$$

where $\sigma_{nl}(\mathbf{R}_1, \mathbf{R}_2, ..., \mathbf{R}_N)$ is a 3×3 shielding tensor whose individual components depend upon both the nature of the electronic state being shielded and the positions of the Rg atoms in the matrix. In actual MC-MCD simulations, it is assumed that the local magnetic field is aligned along the laboratory z axis

$$\mathbf{B}_{local} = B_{local}\mathbf{e}_z \tag{14}$$

which gives

$$H_{Zeeman} = \mu_B B\,(1 - \sigma_{nl})\,(L_z + 2S_z) \tag{15}$$

Different values of B_{local} can be chosen, if desired, to model the effects of slightly different ^2S and ^2P shielding constants σ_{n0} and σ_{n1}. Changes in the direction of B_{local} away from the z axis arising from the tensor character of σ_{nl} can be modeled by preserving the laboratory z axis orientation of the Zeeman perturbation, which is very desirable from the standpoint of matrix element evaluation, and rotating the Rg position vector set through an arbitrary unitary rotation transformation $U\{\mathbf{R}_k\} = \{\mathbf{R}'_k\}$. In any event, it is expected that differences between $\mathbf{B}$ and $\mathbf{B}_{local}$ will be comparatively small for closed shell Rg atoms in their ground ^1S electronic states. Certainly within the chosen MC-MCD simulation restrictions mentioned earlier of neglecting polarization effects and the higher excited states of the Rg atoms, B will not differ much from B_{local}.

E. Diagonalization of the full Hamiltonian matrix in the ^2S and ^2P manifolds

An implementation of degenerate first-order perturbation theory is required to arrive at approximate ^2S and ^2P eigenvalues and eigenvectors of the full M/Rg Hamiltonian given in

Eq. 1. These eigenvalues and eigenvectors contain the effects of the various terms in the interaction Hamiltonian Eq. 3. First-order perturbation theory gives eigenvalues that are correct through first order. The associated eigenvectors are those particular zeroth-order eigenvectors, expressed as orthonormal linear combinations of the zeroth-order eigenvector set $\{|n\,l\,m_l\,s\,m_s\rangle\}$,

$$\Psi_i = |n\,l\,i\rangle = \sum_{m_l=-l,l} \sum_{m_s=-1/2,1/2} C_i^{nlm_l sm_s} \, |n\,l\,m_l\,s\,m_s\rangle \,, \tag{16}$$

$$\langle n\,l\,i'|n\,l\,i\rangle = \delta(i',i), \tag{17}$$

that diagonalize the 2×2 (^2S manifold) or 6×6 (^2P manifold) matrix formed by sandwiching the full Hamiltonian, Eq. 1, within the same uncoupled zeroth-order eigenvector set $\{|n\,l\,m_l\,s\,m_s\rangle\}$; i.e.,

$$\langle n'l'm_l'\,s'm_s'|H|n\,l\,m_l\,s\,m_s\rangle = \langle n'l'm_l'\,s'm_s'|H_M|n\,l\,m_l\,s\,m_s\rangle + \langle n'l'm_l'\,s'm_s'|H_{int}|n\,l\,m_l\,s\,m_s\rangle \,. \tag{18}$$

Both the first-order eigenvalues and the associated zeroth-order eigenvectors are needed for MC-MCD simulations. Since the first matrix element on the right side of Eq. 18 is the zeroth-order matrix element of the free M Hamiltonian, it is automatically diagonal in either the original zeroth-order basis $\{\ |nlm_lsm_s\rangle\ \}$

$$\langle n'l'm_l'\,s'm_s'|H_M|n\,l\,m_l\,s\,m_s\rangle = \varepsilon_{nl}\delta(n',n)\delta(l',l)\delta(m_l',m_l)\delta(s',s)\delta(m_s',m_s) \tag{19}$$

or the new zeroth-order basis $\{|n\,li\rangle\}$

$$\langle n\,l\,i'|H_M|n\,l\,i\rangle = \varepsilon_{nl}\delta(n',n)\delta(l',l)\delta(i',i). \tag{20}$$

Within the ^2S manifold the interaction matrix on the right side of Eq. 18 also is diagonal, thus

$$\Psi_i(^2S) = |n\,0\,i\rangle = \sum_{m_s=-1/2,1/2} C_i^{n00m_s} \left| n\,0\,0\,\frac{1}{2}\,m_s \right\rangle \tag{21}$$

which reduces to

$$\Psi_1(^2S) = \left| n\,0\,0\,\frac{1}{2}\,\frac{1}{2} \right\rangle , \tag{22a}$$

$$\Psi_2(^2S) = \left| n\,0\,0\,\frac{1}{2}\ \ -\frac{1}{2} \right\rangle . \tag{22b}$$

The i index is mapped onto the m_s index one-to-one in this specific case. The final expressions for the ^2S eigenvalues, correct through first order, are obtained by collecting together the matrix elements previously derived for the Rg-Rg, M-Rg, and Zeeman perturbations:

$$\begin{aligned} E_i(^2S) &= \varepsilon_{n0}(^2S) + E_{n0i}(^2S) \\ &= \varepsilon_{n0}(^2S) + U_{Rg-Rg}(^2S) + U_{M-Rg}(^2S) + U_{Zeeman}(^2S) \\ &= \varepsilon_{n0}(^2S) + \sum_{m=1,N} \sum_{m<k} V_{Rg-Rg,X\Sigma}(|\mathbf{R}_m - \mathbf{R}_k|) \\ &\quad + \sum_{m=1,N} \sum_{m<k} V_{M-Rg,X\Sigma}(R_k) + \mu_B B_{local}(2m_s). \end{aligned} \tag{23}$$

In Eq. 23 the eigenvalue convention of Boatz and Fajardo [7] is adopted: E_i is an eigenvalue of a specific ^2S state Ψ_i correct through first order, ε_{n0} is the zeroth order ^2S eigenvalue for the optically active electron of the free M atom, and E_{n0i} is the first-order eigenvalue correction term arising from the interaction Hamiltonian.

To obtain ^2P final state eigenvalues correct through first order

$$E_f(^2P) = \varepsilon_{n1}(^2P) + E_{n1f}(^2P) \tag{24}$$

the first-order eigenvalue set ($E_{n1f}(^2P)$; f = 1,6) must be calculated by diagonalizing the 6×6 ^2P interaction matrix in Eq. 18. The individual matrix elements of this interaction matrix, shown below in Table 1, are obtained by collecting together the matrix elements previously derived for the ^2P Rg-Rg, M-Rg, spin-orbit, and Zeeman perturbations. It should be noted that the U_{Rg-Rg} and the $\langle V_0 \rangle_{M-Rg}$ perturbations are diagonal perturbations in this 6×6 matrix and can be separated from the 6×6 matrix eigenvalue problem as illustrated by Boatz and Fajardo in their Eqs. (6) and (8) [7]. The associated final state ^2P eigenvectors that diagonalize this matrix, are

$$\Psi_f(^2P) = |n\,1\,f\rangle = \sum_{m_1=-1,1} \sum_{m_s=-1/2,1/2} C_f^{n1m_1\,\frac{1}{2}\;m_s} \left| n\,1\,m_1\,\frac{1}{2}\,m_s \right\rangle, \tag{25}$$

where $f = 1, 6$ and

$$\langle n\,1\,f' | n\,1\,f \rangle = \delta(f', f). \tag{26}$$

F. $^2S \rightarrow {}^2P$ transition energies and transition moment integrals for M/Rg MCD spectroscopy

The combined effects of the Rg-Rg, M-Rg, spin-orbit, and Zeeman perturbations on the optically active electron of a M/Rg system act to split the ground ^2S manifold into two energetically distinct states $\{\Psi_i;\, i = 1, 2\}$ and the excited ^2P manifold into six energetically distinct states $\{\Psi_f;\ f = 1, 6\}$. The specific characteristics of the ^2S and ^2P eigenvalues and their associated eigenvectors are dependent upon the particular Rg configuration $\{\mathbf{R}_1, \mathbf{R}_2, ..., \mathbf{R}_N\}$ within which the problem is solved. Thus, for a given Rg configuration $\{\mathbf{R}_1, \mathbf{R}_2, ..., \mathbf{R}_N\}$ and magnitude of the magnetic field, up to 12 energetically and optically distinct transitions may be identified within the manifold-to-manifold $^2S \rightarrow {}^2P$ transition of the M/Rg system. The transition energies of these 12 $^2S \rightarrow {}^2P$ transitions are given as

$$h\nu_{fi} = E_f(^2P) - E_i(^2S) \tag{27}$$

where $i = 1, 2$ and $f = 1, 6$. The Rg-Rg interaction energy terms cancel in Eq. 27 since $U_{Rg-Rg}(^2P) = U_{Rg-Rg}(^2S) = U_{Rg-Rg}$.

Electronic transitions involving the optically active electron of a M/Rg system are well described as electric dipole transitions. In MCD spectroscopy, each of the 12 transitions may be induced to a greater or lesser extent by either LCP or RCP light interacting with the M/Rg system in the electric dipole limit and tuned to the particular transition energy $h\nu_{fi}$. Thus, both LCP and RCP electric dipole transition moment integrals must be computed for each of the 12 possible combinations of initial and final states, i.e., 24 transition moment integrals, 12 for LCP light and 12 for RCP light, are needed to describe the MCD spectrum of a $^2S \rightarrow {}^2P$ transition in M/Rg system in a particular Rg configuration $\{\mathbf{R}_1, \mathbf{R}_2, ..., \mathbf{R}_N\}$; i.e.,

$$\left\langle \Psi_f(^2P) | O_{LCP} | \Psi_i(^2S) \right\rangle \tag{28a}$$

$$\left\langle \Psi_f(^2P) | O_{RCP} | \Psi_i(^2S) \right\rangle \tag{28b}$$

where $i = 1, 2$ and $f = 1, 6$. O_{LCP} and O_{RCP} are the electric dipole transition operators for LCP and RCP light in Eqs. 28a and 28b. The electric dipole moment operator $\mathbf{m}$ of the M/Rg system is, to a very good initial approximation, determined by the position $r = (x, y, z)$ and charge $-e$ of the optically active electron. The Rg atoms are electrically

neutral and their contributions to the dipole moment can be neglected if polarization effects are assumed to be small. The M+ core is positioned at the origin of the chosen coordinate system and thus does not contribute to the expression for the dipole moment at this level of approximation. i.e.,

$$\mathbf{m} = \sum_i q_i r_i = -e\mathbf{r} + e\mathbf{0} = -e(x\mathbf{e}_x + y\mathbf{e}_y + z\mathbf{e}_z) + e(0\mathbf{e}_x + 0\mathbf{e}_y + 0\mathbf{e}_z)$$
$$= -e(x\mathbf{e}_x + y\mathbf{e}_y + z\mathbf{e}_z). \tag{29}$$

However, the optically active electron at position $\mathbf{r}$ will induce a slight polarization in the M^+ core and the Rg matrix. This polarization can be represented as a small negative electrostatic image charge $-q'$ at $-\mathbf{r}$. Thus, polarization effectively reduces the charge of the optically active electron to

$$-e' = -e + q' \tag{30}$$

where $|-e'| < |-e|$. and the dipole moment operator of the M/Rg system becomes

$$\mathbf{m} = -e'\mathbf{r} = -e'(x\mathbf{e}_x + y\mathbf{e}_y + z\mathbf{e}_z). \tag{31}$$

While it can be argued that the image charge $-q'$ (and hence $-e'$) is not, strictly speaking, a constant, but will exhibit both a radial dependence (i.e., different q' for small r vs. large r) and angular dependence arising from the specific positions of the Rg atoms $(\mathbf{R}_1, \mathbf{R}_2, ..., \mathbf{R}_N)$ in the M/Rg system, these effects are neglected at this level of the theory. Within the Piepho and Schatz unit vector conventions for LCP and RCP light [9]

$$\pi_{LCP} = 2^{-1/2}(\mathbf{e}_x - i\mathbf{e}_y) \tag{32a}$$
$$\pi_{RCP} = 2^{-1/2}(\mathbf{e}_x + i\mathbf{e}_y) \tag{32b}$$

the LCP and RCP electric dipole moment operators for the M/Rg system become

$$O_{LCP} = \mathbf{m} \cdot \pi^*_{LCP} = -e'2^{-1/2}(x + iy) = e'(4\pi/3)^{1/2}Y_{11}(\theta, \phi)r, \tag{33a}$$
$$O_{RCP} = \mathbf{m} \cdot \pi^*_{RCP} = -e'2^{-1/2}(x - iy) = -e'(4\pi/3)^{1/2}Y_{1-1}(\theta, \phi)r. \tag{33b}$$

Since each of the $\Psi_i(^2S)$ and $\Psi_f(^2P)$ states is expressed in terms of the uncoupled zeroth-order angular momentum eigenvector set $\{|nlm_l sm_s\rangle\}$ (see Eqs. 16 and 25), the specific form of the transition moment integrals given in Eqs. 33a and 33b may be the determined by

evaluating integrals

$$\langle n\, l' m_l'\, s' m_s' | O_{LCP} | n l m_l\, s m_s \rangle = \langle n l' m_l' 1/2 m_s' | O_{LCP} | n001/2 m_s \rangle = f\delta(m_l', 1)\delta(m_s', m_s), \tag{34a}$$

$$\langle n\, l' m_l'\, s' m_s' | O_{RCP} | n l m_l s m_s \rangle = \langle n l' m_l' 1/2 m_s' | O_{RCP} | n001/2 m_s \rangle = -f\delta(m_l', -1)\delta(m_s', m_s) \tag{34b}$$

where

$$f_{LCP} = f = (e'[4\pi/3]^{1/2}) \langle n1|r|n0\rangle \langle Y_{11}|Y_{11}|Y_{00}\rangle = (e'[3]^{-1/2}) \langle n1|r|n0\rangle \tag{35a}$$

$$f_{RCP} = -f = (-e'[4\pi/3]^{1/2}) \langle n1|r|n0\rangle \langle Y_{1-1}|Y_{1-1}|Y_{00}\rangle = (e'[3]^{-1/2}) \langle n1|r|n0\rangle \tag{35b}$$

Eqs. 34a and 35a express the fact that an LCP electric dipole transition acts on the orbital angular momentum component of the uncoupled wave function, increasing both l and m_l by one unit while leaving s and m_s unchanged. The corresponding RCP electric dipole transition described in Eqs. 34b and 35b also acts on the orbital angular momentum in the uncoupled wave function, increasing l by one unit and decreasing m_l by one unit. In Eqs. 35a and 35b f is the magnitude of the evaluated transition moment integral. Note that the value of f is the same for all allowed transitions. By combining the transition moment integral expressions in Eqs. 28, 34, and 35 with the appropriate expressions for $\Psi_i(^2S)$ and $\Psi_f(^2P)$ in the uncoupled basis as given in Eqs. 16,. 17, and 25, final expressions for the contribution to the MCD spectrum by the transition $i \rightarrow f$ at energy $h\nu_{fi}$ can be written:

$$\begin{aligned}\Delta A'(v_{fi}) &= A_{LCP}(\nu_{fi}) - A_{RCP}(\nu_{fi}) \\ &= \alpha\{|\left\langle \Psi_f(^2P)|O_{LCP}|\Psi_i(^2S)\right\rangle|^2 - |\left\langle \Psi_f(^2P)|O_{RCP}|\Psi_i(^2S)\right\rangle|^2\} \\ &= \alpha f^2\{|C_f^{n1,m_l=1,m_s}|^2 - |C_f^{n1,m_l=-1,m_s}|^2) \times [1 + (e^{-2\mu_B B/kT} - 1)\delta(m_s, 1/2)]\end{aligned} \tag{36}$$

where α is a numerical constant that relates the squared transition moment integrals to the absorbances and the initial state index i is associated with $m_s = -1/2$ or $1/2$ in the ^2S manifold. The MCD spectral amplitude at energy $h\nu_{fi}$ for the Rg configuration $\{\mathbf{R}_1, \mathbf{R}_2, ..., \mathbf{R}_N\}$ is seen to be related to differences of squares of selected ^2P eigenvector coefficients computed for that configuration. The term in square brackets on the right side of Eq. 36 is a Boltzmann factor for the ^2S manifold. The Zeeman perturbation splits the energies of the $m_s = -1/2$ and $1/2$ states of the ^2S manifold by a factor of $2\mu_B B$. The $m_s = -1/2$ and $1/2$ states will, therefore, have different thermal populations. This must be accounted for in computing the various contributions to the MCD spectrum.

III. MONTE CARLO SIMULATION OF THE MCD SPECTRUM

The full MCD spectrum for a $^2S \rightarrow {}^2P$ transition in a M/Rg system in a specific Rg configuration $\{\mathbf{R}_1, \mathbf{R}_2, ..., \mathbf{R}_N\}$ is, therefore, a "stick MCD spectrum" consisting of 12 lines, appropriately placed on the x (energy) axis at transition energies $h\nu_{fi}$, whose magnitudes and directions (+ or -) on the y ($\Delta A'$) axis are determined by computing Eq. 36 for all possible choices of i and f. To simulate a real MCD spectrum, many stick MCD spectra, each arising from a different Rg configuration, are averaged together using a simple binning (histogram) technique based upon the original Metropolis et al. algorithm [24] exactly as implemented by Boatz and Fajardo for the case of electronic absorption spectroscopy [7]. A MC-MCD simulation begins by choosing an initial Rg configuration $\{\mathbf{R}_1, \mathbf{R}_2, ..., \mathbf{R}_N\}_{initial}$, typically , representing an idealized trapping site (e.g., a single substitutional site with O_h symmetry). The MC energy optimization scheme operates in the ^2S ground state manifold. At this stage, the very small Zeeman perturbation of the ^2S manifold is neglected. MCD stick spectra arising from more favorable configurations are weighted more heavily in the averaging process than those arising from the less favorable configurations. In actual practice, the LCP and RCP contributions to the MCD spectrum appearing in Eq. 36 are accumulated and stored separately. This allows the electronic absorption spectrum to be recovered from the MC-MCD simulation as [9]

$$A' = A = \frac{1}{2}[A'_{LCP} + A'_{RCP}]. \tag{37}$$

Eq. 37 expresses the fact that the electronic absorption spectra of M/Rg systems are essentially unaffected by the application of an external magnetic field.

A. Orientational averaging in MC-MCD simulations

In an MCD experiment, the propagation direction of the light, which is always parallel to the **B** vector, rigorously defines the laboratory frame z axis. The laboratory frame x and y axes are set parallel to the sapphire deposition window and perpendicular to **B** with the origin at the M nucleus. All Rg positions, eigenvectors, and selection rules are described with respect to this laboratory frame. To model the effects of arbitrary Rg lattice orientation relative to the laboratory frame, the 6×6 ^2P matrix listed in Table 1 is separated into

M/Rg and spin-orbit + Zeeman matrices

$$[M/Rg + SO + Zeeman] = [M/Rg] + [SO + Zeeman]. \tag{38}$$

Arbitrary orientations of the Rg matrix relative to the laboratory frame can be modeled by re-writing Eq. 38 as

$$[M/Rg + SO + Zeeman] = [U][M/Rg][U]^{-1} + [SO + Zeeman] \tag{39}$$

where U is an arbitrary randomly generated unitary rotation matrix (e.g., an Eulerian rotation matrix). The MC-MCD simulation process is carried out as before using Eq. 39 rather than Eq. 38.

B. Lattice temperature and magnetic temperature in MC MCD simulations

Temperature effects appear in two distinct places in MC-MCD simulations. A lattice temperature must be specified for the MC simulation process. It may be argued that a proper representation of quantum mechanical zero point vibrational motions of the M/Rg lattice at temperature T requires the classical MC simulation to be carried out at a classical lattice temperature $T' > T$ [8]. However, a temperature for the Boltzmann factor of the Zeeman-split ^2S term also must be included. This magnetic temperature, T_{mag}, always should be the actual system temperature T ($T_{mag} = T$). The MC-MCD simulation code has the option of specifying separate values for the lattice temperature T' and the magnetic temperature T_{mag}. Lawrence and Apkarian discuss the relationship between T' and T in classical MC simulations of doped Rg systems [8]. In practice T' is calibrated to T by comparing the Rg MC equilibrium lattice spacing (for first and second nearest neighbors) with the experimentally measured values [25]. For Ar at 10 K, the first nearest neighbor analysis predicts a lattice temperature of $31K$, while the second nearest neighbor analysis predicts a slightly lower lattice temperature of $27K$. Consequently a simulation lattice temperature in the vicinity of $30K$ represents the best modeling of the quantum zero point vibrations of the Ar lattice. The Na/Ar system at a magnetic temperature, $T_{mag} = 10K$, a Na ^2P spin-orbit parameter of 17 cm^{-1} (the value for unperturbed atomic Na) is illustrated in Figures 1a and 1b in which are presented the simulated absorption and MCD spectra, respectively, for three different choices of lattice temperature, $T' = 10K$, $30K$ and $45K$.

While the characteristic 3-peaked "triplet" absorption feature and the corresponding down, down, up MCD triplet feature are preserved for all three choices of T'; the spectral breadth increases as T' increases, improving agreement between simulated and experimental spectra. The difference in peak height is due to the fact that the total area under the absorption curve is normalized to 1.0; broader peaks will be shorter.

C. Other important properties of MC-MCD simulations

For the single substitutional site in the Na/Ar system, absorption and MC-MCD simulations correctly reproduce other observed properties of experimental absorption and MCD spectra M/Rg systems. For example, the observed insensitivity of the experimental $^2S \rightarrow {}^2P$ M/Rg triplet absorption feature to the magnetic field strength and T_{mag} is faithfully reproduced in the MC-MCD simulation as shown in Figure 2. Reversal of the magnetic field direction ($\mathbf{B} = B\mathbf{e}_z$ changed to $\mathbf{B} = -B\mathbf{e}_z$) in an MCD experiment has the effect of inverting the MCD spectrum. If the normal MCD spectrum follows a down-down-up pattern, the MCD spectrum with the reversed magnetic field will be the mirror image of the original spectrum with an up-up-down pattern. In Figure 3, it is seen that the MC-MCD simulations of Na/Ar correctly gives an inverted spectrum when $\mathbf{B}$ is replaced with $-\mathbf{B}$. These successes suggest the MC-MCD simulation embodies much of the essential physics of the Na/Ar system and its interaction with external magnetic fields, the perturbing effects of the Rg matrix and electromagnetic radiation. Overall, the MC-MCD simulated Na/Ar absorption and MCD spectra show good qualitative agreement with experimental Na/Ar spectra.

IV. ACKNOWLEDGEMENTS

It is a great pleasure to acknowledge Mario E. Fajardo for his helpful discussions on theory and his insight in making connections between theory and experiment. The Air Force Office of Scientific Research Summer Faculty Research Program (AFOSR-SFRP) and Graduate Student Research Program (AFOSR-GSRP) and the Research Corporation Partners in Science Program are thanked for financial support.

[1] M. E. Fajardo, P. G. Carrick, J. W. Kenney, III. *J. Chem. Phys.*, 94:5812–5825, 1991.

[2] M. E. Fajardo. *J. Chem. Phys.*, 98:110–118, 1993.

[3] S. Tam; M. Fajardo. *J. Chem. Phys.*, 99:854–860, 1993.

[4] R. Corbin; M. Fajardo. *J. Chem. Phys.*, 101:2678–2683, 1994.

[5] T. L. Thompson M. E. Cordonnier M. E. Fajardo, S. Tam. *Chem. Phys.*, 189:361–365, 1994.

[6] P. G. Carrick. Specific impulse calculations of high energy density solid cryogenic rocket propellants. i: Atoms in solid h2. Technical Report PL-TR-93-3014, Phillips Laboratory, Edwards AFB, CA, 1993.

[7] J. Boatz; M. Fajardo. *J. Chem. Phys.*, 101:3472–3487, 1994.

[8] W. G. Lawrence; V. A. Apkarian. *J. Chem. Phys.*, 101:1820–1831, 1994.

[9] S. B. Piepho; P. N. Schatz. *Group Theory in Spectroscopy with applications to Magnetic Circular Dichroism*. Wiley, New York, 1983.

[10] J. Mort F. Luty. *Phys. Rev. Lett.*, 12:45–57, 1964.

[11] C. H. Henry; S. E. Snatterly; C. P. Schlickter. *Phys. Rev.*, 137:A583, 1965.

[12] F. C. Brown J. Mort, F. Luty. *Phys. Rev.*, 137:A566–A573, 1965.

[13] Y. Merle d'Aubinge, A. Roussel. *Phys. Rev. B*, 3:1421–1427, 1971.

[14] P. J. Stephens G. A. Osborne. *J. Chem. Phys.*, 56:609–618, 1972.

[15] J. Hormes; J. Schiller. *Chem. Phys.*, 74:433–439, 1983.

[16] P. A. Lund; D. Smith; S. M. Jacobs; P. N. Schatz. *J. Phys. Chem.*, 88:31–42, 1984.

[17] P. A. Lund, et al. *J. Chem. Phys.*, 90:2608–2615, 1986.

[18] C. Samet; J. L. Rose; B. E. Williamson; P. N. Schatz. *Chem. Phys. Lett.*, 142:557–561, 1987.

[19] M. C. M. O'Brien. *J. Phys. C: Solid State Physics*, 18:4963–4973, 1985.

[20] M. C. M. O'Brien. *J. Chem. Phys.*, 82:3870–3871, 1985.

[21] M. Weissbluth. *Atoms and Molecules*. Academic, New York, 1978.

[22] E. U. Condon and G. H. Shortley. *The Theory of Atomic Spectra*. Cambridge: London, 1963.

[23] J. S. Griffith. *Theory of Transition Metal Ions*. Cambridge: London, 1961.

[24] N. Metropolis, A. W. Rosenbluth, M. N. Rosenbluth, A. H. Teller, E. Teller. *J. Chem. Phys.*, 21:1087, 1953.

[25] H. A. Terrill-Stolper. Theory of the Magnetic Circular Dichroism (MCD) and Electronic

Absorption Spectra of Alkali Metals Matrix Isolated in Cryogenic Rare Gases. I. Master's thesis, New Mexico State University, 1996.

Fig. 1. Comparison of the temperature effects in the (a) absorption and (b) MCD spectra for the case of $SO = 17cm^{-1}$, $B = 1.0\,T$, magnetic temperature, $T_m = 10\,K$, at simulation temperatures of 10, 30, and 45 K

Fig. 2. Absorption spectra with (a) normal and (b) reversed B-fields. 1-atom vacancy, SO = 17 cm^{-1}, and T_{mag} = 6, 8, 10 K. The magnitudes of the B-fields are 1.0 T.

Fig. 3. MCD spectra with (a) normal magnetic field alignment and (b) reversed magnetic field alignment. 1-atom vacancy, SO = 17 cm^{-1}, and T_{mag} = 10 K. The magnitudes of the B-fields are 1.0 T.

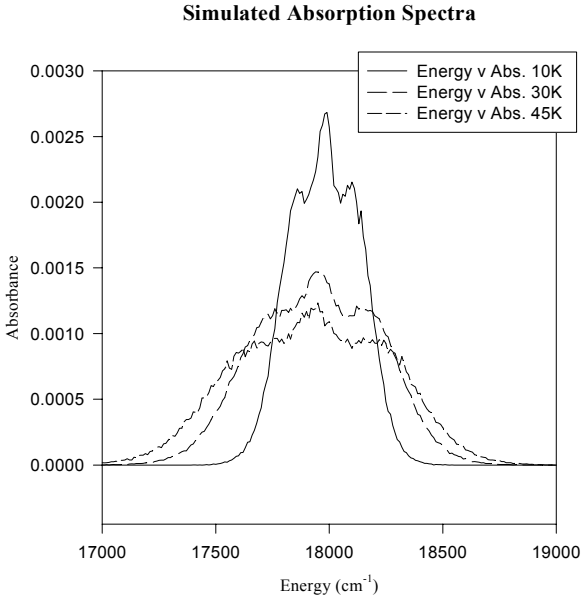

Fig. 1a

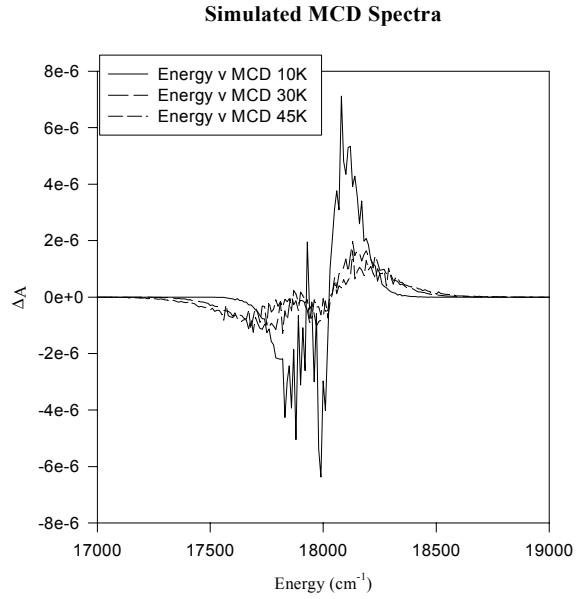

Fig. 1b

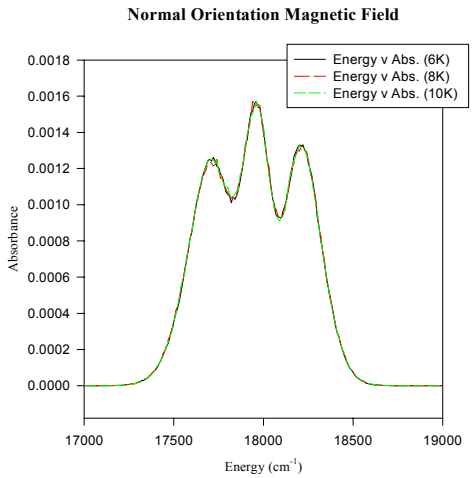

Fig. 2a

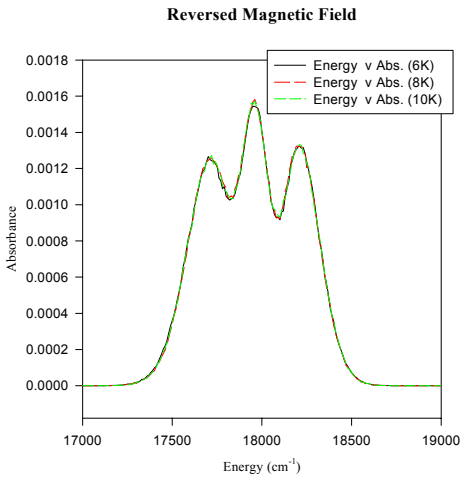

Fig. 2b

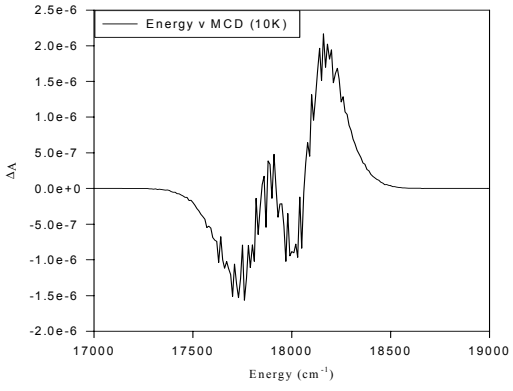

Fig. 3a.

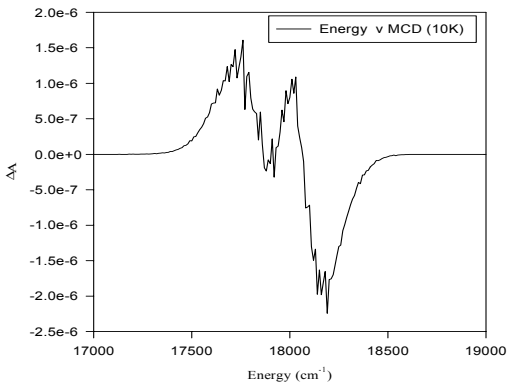

Fig. 3b.

Table 1: Matrix Elements of the $6 \times 6\ ^2P$ Interaction Matrix in the Uncoupled Angular Momentum Representation $|nlm_l sm_s\rangle$

	$\left\vert n11\ \frac{1}{2}\ \frac{1}{2}\right\rangle$	$\left\vert n10\ \frac{1}{2}\ \frac{1}{2}\right\rangle$	$\left\vert n1\ -1\ \ \frac{1}{2}\ \frac{1}{2}\right\rangle$	$\left\vert n11\ \frac{1}{2}\ \ -\frac{1}{2}\right\rangle$	$\left\vert n10\ \frac{1}{2}\ \ -\frac{1}{2}\right\rangle$	$\left\vert n1\ -1\ \ \frac{1}{2}\ \ -\frac{1}{2}\right\rangle$
$\left\langle n11\ \frac{1}{2}\ \frac{1}{2}\right\vert$	$\langle V_0\rangle + \frac{1}{10}\langle V_2\rangle \times \left[-\left(3\cos^2\theta_k - 1\right)\right] + \frac{1}{2}\zeta_{nl} + 2\mu_B B + U_{Rg-Rg}$	$\frac{1}{10}\langle V_2\rangle \times \left[-3\sqrt{2}\sin\theta_k \cos\theta_k e^{-i\phi_k}\right]$	$\frac{1}{10}\langle V_2\rangle \times \left[-3\sin^2\theta_k e^{-2i\phi_k}\right]$			
$\left\langle n10\ \frac{1}{2}\ \frac{1}{2}\right\vert$	$\frac{1}{10}\langle V_2\rangle \times \left[-3\sqrt{2}\sin\theta_k \cos\theta_k e^{i\phi_k}\right]$	$\langle V_0\rangle + \frac{1}{10}\langle V_2\rangle \times 2\left(3\cos^2\theta_k - 1\right) + \mu_B B + U_{Rg-Rg}$	$\frac{1}{10}\langle V_2\rangle \times \left[3\sqrt{2}\sin\theta_k \cos\theta_k e^{-i\phi_k}\right]$	$\frac{1}{\sqrt{2}}\zeta_{nl}$		
$\left\langle n1\ -1\ \ \frac{1}{2}\ \frac{1}{2}\right\vert$	$\frac{1}{10}\langle V_2\rangle \times \left[-3\sin^2\theta_k e^{2i\phi_k}\right]$	$\frac{1}{10}\langle V_2\rangle \times \left[3\sqrt{2}\sin\theta_k \cos\theta_k e^{i\phi_k}\right]$	$\langle V_0\rangle + \frac{1}{10}\langle V_2\rangle \times \left[-\left(3\cos^2\theta_k - 1\right)\right] - \frac{1}{2}\zeta_{nl} + U_{Rg-Rg}$		$\frac{1}{\sqrt{2}}\zeta_{nl}$	
$\left\langle n11\ \frac{1}{2}\ \ -\frac{1}{2}\right\vert$		$\frac{1}{\sqrt{2}}\zeta_{nl}$		$\langle V_0\rangle + \frac{1}{10}\langle V_2\rangle \times \left[-3\cos^2\theta_k - 1\right] - \frac{1}{2}\zeta_{nl} + U_{Rg-Rg}$	$\frac{1}{10}\langle V_2\rangle \times \left[-3\sqrt{2}\sin\theta_k \cos\theta_k e^{-i\phi_k}\right]$	$\frac{1}{10}\langle V_2\rangle \times \left[-3\sin^2\theta_k e^{-2i\phi_k}\right]$
$\left\langle n10\ \frac{1}{2}\ \ -\frac{1}{2}\right\vert$			$\frac{1}{\sqrt{2}}\zeta_{nl}$	$\frac{1}{10}\langle V_2\rangle \times \left[-3\sqrt{2}\sin\theta_k \cos\theta_k e^{i\phi_k}\right]$	$\langle V_0\rangle + \frac{1}{10}\langle V_2\rangle \times \left[2\left(3\cos^2\theta_k - 1\right)\right] - \mu_B B + U_{Rg-Rg}$	$\frac{1}{10}\langle V_2\rangle \times \left[3\sqrt{2}\sin\theta_k \cos\theta_k e^{-i\phi_k}\right]$
$\left\langle n1\ -1\ \ \frac{1}{2}\ \ -\frac{1}{2}\right\vert$				$\frac{1}{10}\langle V_2\rangle \times \left[-3\sin^2\theta_k e^{2i\phi_k}\right]$	$\frac{1}{10}\langle V_2\rangle \times \left[3\sqrt{2}\sin\theta_k \cos\theta_k e^{i\phi_k}\right]$	$\langle V_0\rangle + \frac{1}{10}\langle V_2\rangle \times \left[-\left(3\cos^2\theta_k - 1\right)\right] - \frac{1}{2}\zeta_{nl} - 2\mu_B B + U_{Rg-Rg}$